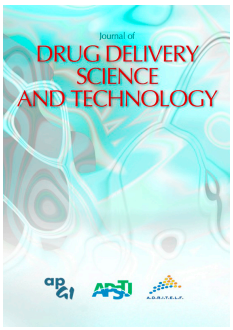

Preparation, Physicochemical and Biopharmaceutical Characterization of Oxcarbazepine-loaded Nanostructured Lipid Carriers as Potential Antiepileptic Devices

S. Scioli Montoto, G. Muraca, M. Di Ianni, M. Couyoupetrou, G. Pesce, G.A. Islan, C.Y. Chain, M.E. Vela, M.E. Ruiz, A. Talevi, G.R. Castro

PII: S1773-2247(21)00150-7

DOI: https://doi.org/10.1016/j.jddst.2021.102470

Reference: JDDST 102470

To appear in: *Journal of Drug Delivery Science and Technology*

Received Date: 24 November 2020

Revised Date: 23 February 2021

Accepted Date: 3 March 2021

Please cite this article as: S. Scioli Montoto, G. Muraca, M. Di Ianni, M. Couyoupetrou, G. Pesce, G.A. Islan, C.Y. Chain, M.E. Vela, M.E. Ruiz, A. Talevi, G.R. Castro, Preparation, Physicochemical and Biopharmaceutical Characterization of Oxcarbazepine-loaded Nanostructured Lipid Carriers as Potential Antiepileptic Devices, *Journal of Drug Delivery Science and Technology*, https://doi.org/10.1016/j.jddst.2021.102470.

Author statement

Scioli Montoto, S., experimental work, statistical analysis, and writing

Muraca, G., experimental work

Di Ianni, M., experimental work, writing

Couyoupetrou, M., experimental work

Pesce, G., experimental design, and funding

Islan, G.A., experimental work, data analysis, Ms. correction, and funding

Chain, C.Y., experimental work, data analysis

Vela, M.E., experimental design, supervision, and Ms. correction

Ruiz, M.E., supervision

Talevi, A., data analysis, supervision, Ms correction, and funding

Castro, G.R., data analysis, supervision, Ms correction, and funding

Characterization & in vitro release

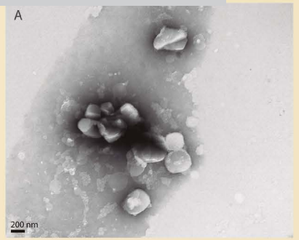

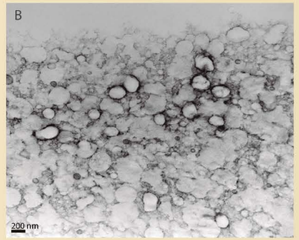

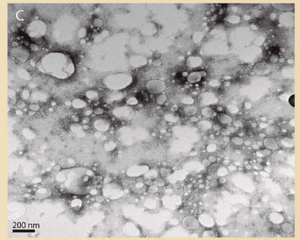

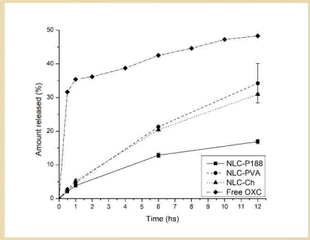

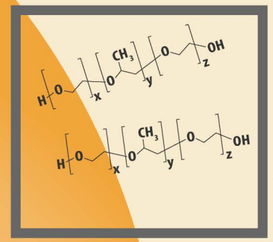

Basic NLC with Poloxamer P188

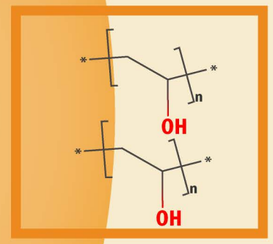

+ PVA Coating

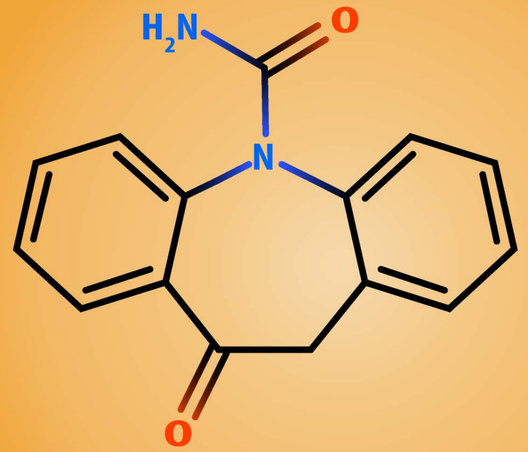

Oxcarbazepine NLC

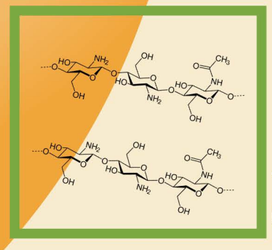

+ Chitosan Coating

Cell permeability

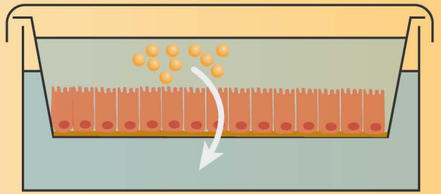

Blood-brain barrier

Binding interaction with proteins

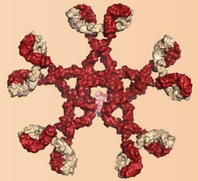

Ig M

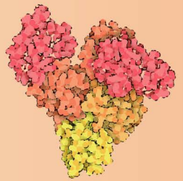

Bovine Suerum Albumin

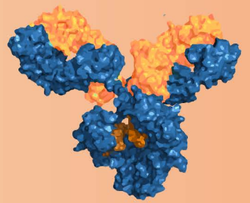

Ig G

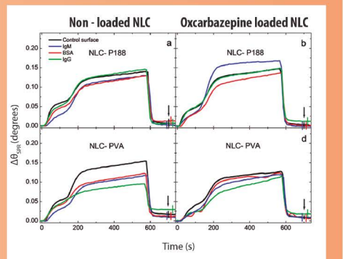

Preparation, Physicochemical and Biopharmaceutical Characterization of Oxcarbazepine-loaded Nanostructured Lipid Carriers as Potential Antiepileptic Devices

Scioli Montoto, S.[a]; Muraca, G.[a,b]; Di Ianni, M.[a]; Couyoupetrou, M.[a,b]; Pesce, G.[b]; Islan, G.A.[c]; Chain, C.Y.[d]; Vela, M.E.[d]; Ruiz, M.E.[a]; Talevi, A.[a*]; and Castro, G.R.[c,e*]

[a] *Laboratorio de Investigación y Desarrollo de Bioactivos (LIDeB), Departamento de Ciencias Biológicas, Facultad de Ciencias Exactas, Universidad Nacional de La Plata (UNLP), Calle 47 y 115 (B1900AJI), La Plata, Buenos Aires, Argentina.*

[b] *Departamento de Farmacología, Instituto Nacional de Medicamentos (INAME), Administración Nacional de Medicamentos, Alimentos y Tecnología Médica (ANMAT), CABA, Buenos Aires, Argentina.*

[c] *Laboratorio de Nanobiomateriales, CINDEFI, Departamento de Química, Facultad de Ciencias Exactas, Universidad Nacional de La Plata (UNLP) -CONICET (CCT La Plata), Calle 47 y 115, (B1900AJI), La Plata, Buenos Aires, Argentina.*

[d] *Instituto de Investigaciones Fisicoquímicas Teóricas y Aplicadas (INIFTA), CONICET-UNLP, CC 16 Suc 4, La Plata, 1900 Buenos Aires, Argentina.*

[e] Max Planck Laboratory for Structural Biology, Chemistry and Molecular Biophysics of Rosario (MPLbioR, UNR-MPIbpC). Partner Laboratory of the Max Planck Institute for Biophysical Chemistry (MPIbpC, MPG). *Centro de Estudios Interdisciplinarios* (CEI), *Universidad Nacional de Rosario*, Maipú 1065, S2000 Rosario, Santa Fe, Argentina.

*Corresponding authors: Prof. Guillermo R. Castro
E-mail: gcastro@cei-mplbior.unr.edu.ar

Prof. Alan Talevi
E-mail: atalevi@biol.unlp.edu.ar
Tel./fax: +542214235333 ext 41

Preparation, Physicochemical and Biopharmaceutical Characterization of Oxcarbazepine-loaded Nanostructured Lipid Carriers as Potential Antiepileptic Devices

Abstract

Epilepsy is the second most common chronic central nervous system disorder. Oxcarbazepine (OXC) is an antiepileptic drug with low solubility in aqueous media but is used for the treatment of both focal and generalized seizures. Studies of OXC encapsulation in nanostructured lipid carriers (NLCs) composed of cetyl palmitate and oleic acid coated with polyvinyl alcohol (PVA) or chitosan (Ch) to obtain nanoparticles with negative and positive surface charge, respectively, are reported. All NLCs displayed 97%-98% OXC encapsulation efficiency, 14.5%-14.6% drug loading, 121.8 to 212.3 nm size range, and polydispersity indexes between 0.248 and 0.282 nm, depending on their composition. The homogeneity of the NLCs was confirmed by electron microscopy. The OXC release from the NLCs was analyzed by Higuchi, Baker-Londsdale, and Korsmeyer-Peppas structured models. The Korsmeyer-Peppas model provides the best data fit (R^2> 0.98), and n> 0.58, suggesting a mechanism driven by non-Fickian molecular release. *In vitro* permeability studies using MDCK-MDR1 cells revealed enhanced permeability of the encapsulated drug compared with free OXC. Surface plasmon resonance tested in the presence of BSA, IgG, and IgM, commonly found in human plasma, revealed no interaction with naked and PVA-coated NLCs. These promising results allow considering further *in vivo* studies for efficient delivery of OXC.

Keywords: Oxcarbazepine; Central nervous system (CNS); Biopharmaceutical characterization; Chitosan; Lipid nanoparticles (LNP); Physical characterization.

Introduction

Epilepsies are the second most common chronic central nervous system (CNS) disorder, following dementias. It is estimated that 65 million people today live with epilepsy worldwide [1]. About 80% of global cases of epilepsy come from low- and middle-income countries, where due to economic reasons barely a quarter of the patients receive the required treatment ~~due to~~ [2]. Despite the substantial and successful efforts to find new treatments, with a considerable number of new antiepileptic drugs (AEDs) introduced to the market in the past two decades, around one-third of the patients still fail to control seizures with the available drugs [3]. A large volume of evidence from both patients and animal models indicates that drug resistance in epilepsy is associated with over-expression of ABC transporters (the so-called "transporter hypothesis"), a superfamily of ATP-dependent carriers (*e.g.*, P-glycoprotein) that work in a highly concerted manner with biotransformation enzymes to promote the elimination of xenobiotics from the body [4,5]. Up-regulation of such systems may lead to subtherapeutic levels of their substrates, among them some AEDs. Most recently, the "gene variant" hypothesis has also contemplated genetic causes of drug-resistant epilepsy (*e.g.*, polymorphic variants of drug biotransformation enzymes and/or drug transporters) [6].

Different strategies have been proposed to address the previous issues, among them the use of drug nanocarriers that could "hide" the AEDs from elimination systems, analogous to Trojan horses, and thus increase drug bioavailability [7,8]. Multiple nanocarriers have been studied for such purposes, including polymer and lipid systems [9]. Preclinical studies have shown that the concentration of AEDs in the brain can be improved by encapsulating such active pharmaceutical ingredients in diverse vehicles [10].

Among the different colloidal systems, solid lipid nanoparticles (SLNs) have emerged as promising carriers for the delivery of AEDs and are produced with a solid lipid core stabilized by emulsifiers [11]. Nanostructured lipid carriers (NLCs) appeared as a second-generation of SLNs containing both solid (fat) and liquid (oil) lipids inside the nanoparticle. The addition of the oil into the matrix disrupts the crystal structure of the solid lipid, improving their stability, drug loading, kinetic release, and preventing drug expulsion during storage [12,13]. Both lipophilic and hydrophilic compounds could be loaded into NLCs [14,15], and the surface could be modified to improve their stability and site-specific targeting using Green Chemistry technologies [12,16].

Many nanometric systems could be eliminated through opsonization followed by recognition by macrophages, which can markedly limit the therapeutic activity of the transported drugs and could induce undesirable side effects. This process is activated immediately after the

particles enter in contact with the blood when they undergo decoration with opsonins (*i.e.,* immunoglobulins, complement factors, etc.) that flag them and promote their elimination by the mononuclear phagocytic system [17,18]. Abundant evidence indicates, however, that this phenomenon can be reduced by coating the nanoparticles with different polymeric substances [19]. Polyvinyl alcohol (PVA) and chitosan (Ch) coating could provide increased nanoparticle stability but also changes in the residual surface charge. Ch is a positively charged biopolymer composed of partially deacetylated ß-(1→4) glucosamine and N-acetylglucosamine and, on the other hand, PVA provides the nanoparticles residual negative surface charge.

OXC is a Biopharmaceutical Classification System class II AED used for both focal and generalized seizures, either alone or as add-on therapy. It is, in fact, a prodrug that is rapidly converted into its main metabolite, the active 10-monohydroxy derivative licarbazepine. OXC displays a short half-life of 1 to 5 h [20]. Both OXC and licarbazepine have been reported as P-glycoprotein substrates [21], and thus encapsulation of OXC within pharmaceutical nanocarriers is likely to have a considerable impact on its disposition and pharmacokinetics.

In this sense, kinetic analysis of OXC release from the nanoparticles using structured models could reveal the main characteristic of the drug release system. Some of the typical models used for controlled drug release were postulated by Baker-Londsdale, Higuchi and collaborators, and Korsmeyer-Peppas [22]. Particularly, the Korsmeyer-Peppas structured model is interesting because it allows determining the main release mechanism of the encapsulated drug from the device through the exponential value (n). The Korsmeyer-Peppas kinetic release model for spheres establishes that $n \leq 0.43$ can be associated with a Fickian diffusional mechanism, $0.43 < n < 0.89$ is correlated with non-Fickian drug release, a combination of diffusional, swelling, and erodibility mechanisms, $n= 0.89$ can be associated with the relaxational transport (case II type), and $n> 0.89$ is assigned to super case II.

In previous works the encapsulation of OXC intended for nasal administration, including its formulation as polymeric nanoparticles [23,24] and as emulsomes [25,26], was reported. To the best of our knowledge, SLN/NLC formulations of OXC have not been reported yet. The advantage of these systems, compared to those reported by other authors, is the lack of organic solvents (which can be potentially toxic if they are not eliminated) during the preparation process. Moreover, this type of nanovehicle has been assayed for the related AED carbamazepine (CBZ), with encouraging results, as an improved biodistribution and/or anticonvulsant effect of the drug has been previously reported [11,27,28]. Therefore, the aim of the present work was the preparation and subsequent physicochemical and *in vitro* biopharmaceutical characterization of OXC-loaded in three NLC systems: naked, coated with

PVA, and Ch. *In vitro* studies included nanoparticle characterization by dynamic light scattering (DLS) and transmission electron microscopy, kinetic drug release and modeling, and permeability studies in the MDCK-MDR1 cell line. Furthermore, the interaction of the prepared formulations with opsonins was analyzed by surface plasmon resonance (SPR).

Materials and methods

Chemicals

Cetyl palmitate (Crodamol CP®, M.P.= 50–53°C) was kindly donated by Croda (Argentina). OXC (98.1% as basis) and bidistilled oleic acid were provided by Saporiti (Buenos Aires, Argentina). Poloxamer 188 (P188, Kolliphor®), polyvinyl alcohol (PVA, MW≈ 13–23 kDa, 98.0% hydrolyzed), medium molecular weight Chitosan (mCh, MW≈ 190–310 kDa, 75%–85% deacetylated), bovine serum albumin (BSA, MW= 66.5 kDa), IgG and IgM antibodies, 11-mercaptoundecanoic acid (MUA), N-hydroxysuccinimide (NHS), ethanolamine hydrochloride, and N-(3-dimethylaminopropyl)-N´-ethyl carbodiimide hydrochloride (EDC) were purchased from Sigma-Aldrich (Buenos Aires, Argentina). Potassium chloride, sodium chloride, sodium dihydrogen phosphate, and disodium hydrogen phosphate were obtained from J. T. Baker (Pasadena, CA, USA). Sodium carbonate was purchased from Biopack (Buenos Aires, Argentina). Commercial gold substrates (SPR102-AU) were obtained from BioNavis (Tampere, Finland). All reagents were of HPLC/analytical grade unless specified otherwise.

Preparation of OXC- NLCs

OXC-loaded NLCs were prepared by melt-emulsification procedures followed by ultrasonication technique [29]. Briefly, 400 mg of cetyl palmitate (Crodamol CP®) was melted ~~into~~ in a water bath at 70 °C and mixed with 60 mg of OXC dissolved in a mixture containing 50 µL of dimethyl sulfoxide (DMSO), 2.0 mL of propylene glycol, and 112 µL of oleic acid. After 30 min, 20 mL of a preheated (70 °C) 3.0% (w/v) Poloxamer 188 (Kolliphor® P188) aqueous solution was ~~were~~ mixed with the lipid/drug phase (2.0%, w/v). The formulation was finally obtained by ultrasonication at 90% amplitude for 30 min. An ultrasonic processor (130 W, Cole-Parmer, USA) equipped with a 3 mm titanium tip was used. The resulting suspension (NLC-P188) was rapidly cooled down to room temperature, and the remaining volume was measured. Two additional formulations (NLC-PVA and NLC-mCh) including coating polymers were prepared, by adding PVA or mCh to the aqueous phase, respectively. In the case of NLC-mCh, the procedure involved the dissolution of 2.0% (w/v) mCh in 0.1% acetic acid (pH= 4.0)

and then preheating to 70 °C before the addition of the polymer to the aqueous phase. Non-loaded control NLCs (*i.e*., without OXC) of each formulation was also prepared.

Particle size, zeta potential, and polydispersity index

The mean diameter and size distribution were measured by DLS (Nano ZS Zetasizer, Malvern Instruments Corp, U.K.) at 25 °C in polystyrene cuvettes with a path length of 10 mm. The zeta potential (ζ) was determined by laser Doppler anemometry using the same equipment. Measurements were performed in 10 mm path length capillary cells, using ultrapure water (Milli-Q®, Millipore, MA, USA). As a dimensionless measure of the size dispersion, the polydispersity index (PI) was determined. All measurements were carried out in triplicate.

Measurement of entrapment efficiency and drug loading

The entrapment efficiency (EE, %) and drug loading (DL, %) of all formulations were determined by measuring the concentration of the nonencapsulated drug in the solution [11]. The final suspension of 500 µL was filtered using 10 kDa cut-off filters (Microcon®, Merck Millipore, Billerica, MA, USA). The concentration of free OXC was then assessed using an HPLC method. The EE and DL were calculated as:

$$EE\ (\%) = \frac{W_{0-}(C_{fr} \times V_f)}{W_0} \times 100 \qquad (1)$$

$$DL\ (\%) = \frac{W_0}{W_{lipid}} \times 100 \qquad (2)$$

where W_0 and W_{lipid} are the initial amounts (in mg) of OXC and lipid added to the formulation, respectively, C_{fr} is the free drug concentration in mg/mL in the ultrafiltrate, and V_f is the final volume (mL) of formulation obtained after ultrasonication.

HPLC analysis

A Dionex Ultimate 3000 UHPLC (Thermo Scientific, Sunnyvale, CA, USA) equipped with a dual gradient tertiary pump (DGP-3000) and a DAD-3000 diode array detector was used for chromatographic analysis. A Lichrosphere® 100 RP-18 (250 mm × 4 mm, 5 µm, Merck KGaA, Darmstadt, Germany) column was used for chromatographic separation. The mobile phase consisted of methanol and KH_2PO_4 buffer (70:30). The system was operated isocratically at a

flow rate of 1.0 mL/min, with detection being performed at 285 nm. The mobile phase was used to dilute the samples, which were then centrifuged at 13,000 xg for 5 min (4 °C) before injection (20 µL). Method validation was carried out through the determination of the precision, specificity, and linearity over the range of expected concentrations. Precision was determined at three different concentrations: 0.1, 20.0, and 50.0 mg/L. The calculated relative standard deviations were below 3% in all cases. The method was specific for the drug in the lipid matrix; no interfering peaks were observed near the OXC retention time. A linear correlation ($p< 0.0001$) was observed in the concentration range of 0.1 – 50.0 mg/L, with a coefficient of determination R^2= 0.997 and a 95% confidence interval of the intercept of [−1.2322 – 0.6447].

Transmission electron microscopy

A ten-fold dilution of each nanoparticle formulation was obtained using ultrapure water; a drop of the resulting dispersion was spread onto a collodion-coated Cu grid (400 mesh). Liquid excess was drained with filter paper. One drop of phosphotungstic acid was added for contrast enhancement. Transmission electron microscopy (TEM) analysis was performed using Jeol-1200 EX II-TEM microscope (Jeol, MA, USA.).

In vitro cell permeability studies

Parental MDR1-transfected Madin–Darby canine kidney (MDCK) epithelial cells were a gentle donation from the Netherlands Cancer Institute (Amsterdam, The Netherlands). Along with Caco-2 cells, MDCK cells are the most broadly used cells to assess drug permeability *in vitro.* Under standard culture conditions, MDCK cells form monolayers of polarized cells and develop tight junctions [30]. Here, MDCK-MDR1 cells expressing human P-gp were selected, so that the observed apparent permeability coefficients (Papp) reflect the contribution of P-gp to drug transport [31]. Cells were grown in 25 cm^2 culture flasks using DMEM with 10% fetal bovine serum, 1% L-glutamine, 1% nonessential amino acids, and penicillin and streptomycin at 37 °C in 5% CO_2 atmosphere. Cells were split twice a week at 70%–80% range confluence in a ratio of 1:20 or 1:30 using Trypsin-EDTA solution (0.25%). Transport assays were performed with cells from passages 19 – 43. Cells were kept at 37 °C in 5% CO_2 and seeded in 6-well Costar Snapwell plates with polycarbonate membrane inserts at a density of 50,000 cells per insert (1.12 cm^2), which is grown for 4 days in the culture medium. The medium was replaced every day. The apical medium volume was 0.5 mL, and the basal volume was 2.0 mL. The transepithelial electrical resistance (TEER, $\Omega.cm^2$) was measured to assess the integrity of the monolayer,

using an epithelial voltammeter (Millicell-ERS; Millipore Corporation). On the day of the experiment, the culture medium was removed, and cells were washed three times with transport medium Hanks' balanced salt solution (HBSS, pH= 7.4; Gibco-BRL, IN, USA). The filter inserts containing the cell monolayers were placed in a using chamber and kept at 37 °C under constant gassing with carbogen. Test formulations were NLC-P188, NLC-PVA, NLC-mCh prepared in transport media to a final concentration of 1.0 µM. Then 4.0 mL of each formulation was added to the apical chamber. At 20, 40, 60, 80, 100, and 120 min, samples (400 µL) were taken from the basolateral compartment followed by the addition of 400 µL of HBSS. A solution of free OXC was used as control. P_{app} was calculated by using the following equation:

$$P_{app} = \frac{1}{A.C_0} \times {}^{dQ}/_{dt} \qquad (3)$$

where *A* is the membrane surface area (1.12 cm^2), C_0 is the initial concentration in the donor compartment at t= 0, and *dQ/dt* is the amount of drug transported within a given time.

In vitro release studies

Dissolution studies of the OXC released from nanoparticles were performed in ~~a~~ rotating paddle apparatus [32] (Vision Classic 6, Hanson Research, Chatsworth, CA, USA) at 100 rpm using 500 mL of KH_2PO_4 buffer (pH= 6.8) as dissolution media. Such dissolution media was previously filtered and deaerated with a 0.45 µm nylon filter. The heating temperature was established at 37.0 ± 0.5 °C. A suitable volume of each formulation (5.0 mL) was placed in dialysis membranes (MWCO= 10 kDa), which were prehydrated for 24 h, and submerged in a vessel. Pure OXC solution at a similar concentration was used as a control. Samples were taken at regular intervals of time and immediately centrifuged at 2200 xg for 24 h. The quantity of the released drug was determined spectrophotometrically at λ= 285 nm (Helios Beta spectrophotometer, Thermo Fisher Scientific, Waltham, MA, USA). Experiments were performed in duplicate; the mean values were used for data analysis. Different mathematical models of drug release were considered to describe the drug dissolution profile from NLC formulations [33].

SPR Measurements

Single thiol self-assembled monolayers (SAMs) were obtained by overnight incubation of the

gold substrates in 50 μM MUA ethanolic solution at room temperature. The as-prepared surfaces were washed with Milli-Q® water and dried in a stream of nitrogen before SPR measurements.

Experiments were performed with an SPR Navi® 210A (BioNavis, Tampere, Finland) instrument at 22 °C using an incident laser of λ= 785 nm and a flow rate of 10 μL/min. The working mode was "in parallel" by immobilizing blood plasma proteins (BSA, IgG, or IgM) in one flow cell of the sensor chip and keeping the other fluidic cell as a control surface without protein. Immobilization of the proteins to the single SAMs was performed by the carbodiimide coupling reaction [34]. Activation of the MUA-carboxyl groups on the surface was implemented with a mixture of 0.1 M EDC and 0.1 M NHS to give reactive succinimide esters. Then 10 mM sodium acetate solutions of 50 µg/mL IgG (pH= 4.6), 100 μg/mL BSA (pH= 4.0) or 20 μg/mL IgM (pH= 4.0) were injected through fluidic cell 1 in three different individual experiments. The esters reacted spontaneously with primary amine groups of the proteins. The immobilization process finished by blocking the remaining succinimide esters with 1.0 M ethanolamine (pH= 8.5). An identical procedure of carbodiimide coupling reaction, but flowing buffer solution instead of protein solution, was performed for the control assay (fluidic cell 2).

To monitor the interaction of NPs with the immobilized proteins, a ten-fold dilution of NLC formulations in PBS (pH= 7.4) was injected for 10 min onto the sensor chip followed by a regeneration step with 1% Triton X-100. The SPR signal assigned to each NLC solution corresponded to the plateau of the SPR response in the time between the end of the NLC injection and the start of the regeneration step (around 730 s of each cycle). All sensorgrams are displayed as mean ± SD from 3 independent experiments.

Results and discussion

Synthesis and characterization of NLC formulations

Different NLC formulations were prepared by the ultrasonication method using a common lipid core composed of cetyl palmitate and oleic acid as liquid oil, as well as PVA or mCh as coating polymers. Due to the low solubility of OXC in a wide range of solvents [35], it was partially dissolved in a minimal volume of 0.25% (v/v) DMSO, which is below the maximum allowable concentration limit established by the FDA [36]. Dissolution was completed with propylene glycol. The resulting mixture was incorporated into the melted lipid phase before preparation. The composition of different NLCs is shown in **Table 1.**

Table 2 summarizes the main properties of the NLCs. All NLC formulations displayed a high EE (%) ranging 97%-98% and DL (%) between 14.5% and 14.6%. All formulations are expected to

have a similar encapsulation performance because all NLCs contain the same lipid core. The high encapsulation performance relates to the nature of the NLC systems, where the drug is highly located in the interstices generated by the liquid lipid component of the oleic acid core, which alters the reticular crystalline structure of the solid lipid (in this case, cetyl palmitate) [37]. It is worth mentioning that the drug loads of the herein reported systems are much higher than those of previously reported polymeric nanoparticles encapsulating OXC [22, 23].

The particle size of the NLCs ranges between 121.8 and 212.3 nm; the increase in particle size is directly correlated with the MW of the coating polymer, as expected. The residual positive charge of mCh, which results in electrical repulsion between the polymeric chains, also contributes to size expansion. The PI of the obtained nanoparticles ranged between 0.248 and 0.282 (**Table 2**), verifying, in all cases, the small polydispersion of the NLC solutions [38,39], which suggests a monomodal dispersion that is optimal for pharmaceutical applications. Concerning the surface charge of the formulations, NLC-P188 and NLC-PVA appear to be slightly negative (**Table 2**), which is an interesting feature to maintain their stability and avoid potential aggregations, added to the fact that the use of the nonionic surfactant P188 enhances nanoparticle stability by steric hindrance [40]. This result is in agreement with works reported elsewhere [41,42]. On the other hand, a switch to a positive surface for nanoparticles coated with mCh was observed (NLC-mCh), a feature that makes them potentially useful for alternative administration routes of AEDs such as intranasal administration, in which the mucoadhesive properties of the particles are highly required [43]. The positive charge conferred by mCh coating could also be useful for a passive targeting strategy to overcome the blood-brain barrier by adsorptive-mediated transport [44,45].

TEM analysis

The size and morphological structure of the three different NLC formulations were evaluated by TEM and analyzed using ImageJ software. Images obtained by this methodology showed spherical shape with a mean particle size (± SD) of 120 ± 32 nm, 153 ± 12 nm, and 212 ± 24 nm for NLC-P188, NLC-PVA, and NLC-mCh, respectively. These results are in the order of those obtained by DLS (**Table 2)**. **Figure 1** shows the images obtained by TEM and used for the mean particle size analysis. These results are in agreement with previous reports where it is shown that DLS measurements could be similar to those obtained by TEM when using the DLS number instead of intensity [46].

Permeability studies

The calculated Papp for the three assayed nanosystems ranged between 0.0212 (+/-0.01), 0.0186 (+/-0.01), and 0.0137 (+/-0.006) cm s^{-1} for NLC-P188, NLC-PVA, and NLC-mCh, respectively. These NLC Papp values are significantly different from the estimated Papp for the OXC solution, which was 0.0006 (+/-0.0004) cm s^{-1} (Kruskal-Wallis test followed by nonparametric pairwise comparisons, 0.05 significance level [47]). This result suggests that the encapsulated drug could be cross the MDCK-MDR1 cell monolayer. Consequently, the delivery of OXC in NLCs has been efficacious to circumvent MDR1-mediated efflux and significantly enhances the permeability of the drug in the *in vitro* permeability studies. An inverse correlation between the size of the nanosystem and the permeability coefficient was observed, as expected.

These results are in agreement with previously published ones, according to which the permeability of OXC across cell monolayers, as *in vitro* models of the BBB, is enhanced by its encapsulation into a nanosystem [23]. A similar result was previously reported by our group for NLCs containing the AED carbamazepine [11].

In vitro release studies

The *in vitro* OXC release profiles from the nanocarriers are shown in **Figure 2**. In comparison with free OXC, all NLCs showed a kinetically controlled release of OXC. The drug release achieved by NLC-PVA and NLC-mCh was ~~is~~ approximately twice compared to NLC-P188 after 12 h incubation. In decreasing order, the drug release performance was NLC-PVA (34.2%) > NLC-mCh (30.9%) > NLC-P188 (16.9%). According to the observed profiles, the data were analyzed with three mathematical models: Higuchi, Korsmeyer-Peppas, and Baker-Lonsdale [48]. The goodness of fit measures for the three models is presented in **Table 3**.

The model developed by Korsmeyer and Peppas was the best fit for the data for all the formulations (**Table 3**), and thus the parameters and their standard error were calculated (**Table 4**). In this model, k_{KP} is a constant incorporating structural and geometric characteristics of the drug dosage form, and n is the release exponent, indicative of the drug release mechanism [49]. All the estimations were highly significant, but no statistical differences ($p > 0.05$) were found among formulations either in terms of k_{KP} or n. The three formulations displayed exponential values (n) in the range of 0.58 to 0.76, which are indicative of a non-Fickian or anomalous transport from spherical devices. In this case, the mechanism of drug release is governed by diffusion and swelling of the coating. In purely polymeric devices, the simultaneous rearrangement of the polymeric chains and the diffusion process could cause time-dependent anomalous effects [50]. These results show the particular relevance of

swelling for those nanosystems in the presence of polymeric coatings, which positively contribute to the release of the OXC from the nanoparticles to the surrounding environment. The observed percentage release "order" was NLC-PVA > NLC-mCh> NLC-P188, which provides further evidence of the role of the coatings in drug release kinetics. The effect of polymers on NLC structure was previously reported in other works of our group [16], where it was observed, by X-ray diffraction, that the addition of a chitosan cover, decreases the diffraction pattern signals corresponding to β and β' lipid polymorphic structure, which could suggest that this polymer could have an interaction with the lipid components and modify the structure of the crystalline surface of NLC [51]. This effect could explain the differences in the release profiles of OXC in the presence of coating polymers.

The OXC release profiles observed in the current study are very similar to those reported previously from emulsomes[24], which were also assayed and improved *in vivo* drug bioavailability. In contrast, OXC release profiles from NLCs indicated a delayed and sustained release compared with previous data published elsewhere [22].

The drug release behavior discussed above-involving release dependence on diffusion, swelling, and the lack of evidence of burst release in all SLNs studied could indicate that the drug was incorporated into the lipid matrix since burst release is associated with fast release and the drug enrichment of nanoparticles surface [52]. In a previous work carried out by our group, the drug carbamazepine was incorporated into the lipid matrix of solid lipid nanoparticles [53]. The similarity that this drug has with oxcarbazepine in terms of its lipophilicity and molecular structure could support this hypothesis. However, more studies are required for further understanding of the system.

SPR sensor chip modification with blood plasma proteins

BSA, IgG, and IgM were covalently immobilized onto the SPR chip covered with EDC/NHS-activated single MUA SAMs. The immobilization was carried out inside the SPR device and ~~it~~ was monitored by the shift of the SPR angle. Mean angular shifts ($\Delta\theta_{SPR}$) and the corresponding protein surface coverage (Γp), calculated through the Feijter equation, together with the hydrodynamic diameters (D_h) and molecular weights (MW) employed to calculate the close-packed coverage (Γp*), are listed in **Table 5**. According to these estimations, the surface coverage for BSA, IgG, and IgM was 31%, 15%, and 28% (considering a close-packed array as 100% of coverage) respectively, which is compatible with an adequate protein - NP interaction in terms of the availability of capturing sites in the immobilized molecules. Because of these data, proteins were successfully immobilized onto the activated MUA SAMs.

SPR measurement of NLC-protein interactions

Considering that the surface coverage for BSA, IgG, and IgM ranges 15%-31% of the close-packed array (**Table 5**), it can be assumed that both nanocarrier-protein and nanocarrier-bare chip surface interactions can occur on the chip surface. To cover these possible interactions, parallel SPR experiments were performed by immobilizing proteins in one flow cell and keeping the other cell as a control surface without protein.

Representative SPR sensorgrams resulting from the flow of NLC-P188 or -PVA onto protein-modified chips or control surfaces are shown in **Figure 3**. These NLC formulations showed a negligible interaction in the control experiments as the $\Delta\theta_{SPR}$ that characterizes the surface after the passage of the NPs is essentially the same as before the injection of the NLCs (black curves in **Figure 3**). The $\Delta\theta_{SPR}$ that results after the injection of NLC-P188 or -PVA onto the protein-covered sensor surfaces (blue, red, and green curves in **Figure** 3 for IgM, BSA, and IgG respectively) overlaps with the $\Delta\theta_{SPR}$ that characterizes the interaction of these NLCs and the bare sensor surfaces, indicating that no interaction between NLC-P188 or NLC-PVA and the tested proteins occurs in the experimental conditions. These results are following a negligible immune system clearance of the nanocarriers. The fact that a reduction of plasma protein adsorption is achieved could lead to a decrease in the clearance of nanoparticles by the reticuloendothelial system, and therefore, an increase in the circulation time of the nanoparticles, which would improve their arrival at the site of action [54]. However, this hypothesis should be further investigated by *in vivo* experiments. Strong interaction with the bare sensor surface was observed in the case of mCh nanocarriers (with or without OXC), preventing the evaluation of the NLC-protein interaction using this experimental design, as observed for other Ch-coated nanoparticles [55].

CONCLUSIONS

Three stable NLC formulations containing OXC were successfully prepared, two of which had additional coating polymers. The systems are spherical with a particle size in the range of 120 to 210 nm, depending on the surface charge of the polymer used, and with a small polydispersity index in all of them.

The permeability studies using MDCK-MDR1 cells indicated enhanced permeability of the encapsulated drug in comparison with OXC free OXC. This is an especially relevant result taking into consideration that OXC is an MDR1 substrate, and thus it is subjected to efflux transport. It is hypothesized that encapsulated OXC molecules are hidden from MDR1 copies, resulting in

increased permeability. Considering that overexpression of MDR1 and other ABC transporters has been associated with refractory epilepsy, this is a promising result to further explore the use of nanocarriers to deliver AEDs more efficiently (*e.g.,* by future assessment of our delivery systems *in vivo* models of drug-resistant seizures and/or epilepsy).

In vitro release results showed modified OXC release, compared to nonencapsulated OXC, with an excellent fit to the Korsmeyer-Peppas model. The release exponent suggested a mixed release mechanism driven both by diffusion and by the rearrangement of polymeric chains of the coatings.

In the case of Ch-coated NLC (NLC-mCh), the SPR studies did not yield results that could provide information about the affinity between the nanoparticles and the studied proteins. In contrast, the SPR *in vitro* experiments verified that there was no interaction of NLC-P188 or NLC-PVA with IgM, IgG, or BSA. This fact may have an impact on the circulation times of the formulations in the bloodstream. Due to the complexity and the relative number of plasma proteins, this hypothesis should be confirmed by future *in vivo* studies.

CONFLICT OF INTEREST

The authors confirm that this article's content has no conflicts of interest.

ACKNOWLEDGEMENTS

The authors would like to thank UNLP and CONICET. The present work was supported by Argentine grants from The National Agency of Scientific and Technological Promotion (ANPCyT, PICTs 2016-1109, 2016-0679, 2016-4597, 2017-0359, 2017-2251), CONICET (PIP 0671 and PUE 22920170100100CO), UNLP (National University of La Plata, 11/X729, 11/X878, 11/ X861, 12/X545, 13/X545, 14/X701 and 18/X815) and UNLP Young Scholars Grants. MEV is a member of the research career of CIC PBA. The authors want to thank CRODA Argentina for kindly donating the lipids.

REFERENCES

[1] A.K. Ngugi, C. Bottomley, I. Kleinschmidt, J.W. Sander, C.R. Newton, Estimation of the burden of active and life-time epilepsy: A meta-analytic approach, Epilepsia. 51 (2010) 883–890. https://doi.org/10.1111/j.1528-1167.2009.02481.x.

[2] WHO, WHO | World Health Statistics reports on global health goals for 194 countries, WHO. (2015).

[3] K.D. Laxer, E. Trinka, L.J. Hirsch, F. Cendes, J. Langfitt, N. Delanty, T. Resnick, S.R. Benbadis, The consequences of refractory epilepsy and its treatment, Epilepsy Behav. 37 (2014) 59–70. https://doi.org/10.1016/j.yebeh.2014.05.031.

[4] J. Xiong, D. Mao, L. Liu, Research Progress on the Role of ABC Transporters in the Drug Resistance Mechanism of Intractable Epilepsy, Biomed Res. Int. 2015 (2015) 10. https://doi.org/10.1155/2015/194541.

[5] W. Löscher, H. Potschka, Drug resistance in brain diseases and the role of drug efflux transporters, Nat. Rev. Neurosci. 6 (2005) 591–602. https://doi.org/10.1038/nrn1728.

[6] M. Couyoupetrou, M. E. Gantner, M. E. Di Ianni, P. H. Palestro, A. V. Enrique, L. Gavernet, M. E. Ruiz, G. Pesce, L. E. Bruno-Blanch, A. Talevi, M.E. Gantner, M.E. Di Ianni, P.H. Palestro, A. V Enrique, L. Gavernet, M.E. Ruiz, G. Pesce, L.E. Bruno-Blanch, A. Talevi, Computer-Aided Recognition of ABC Transporters Substrates and Its Application to the Development of New Drugs for Refractory Epilepsy, Mini-Reviews Med. Chem. 17 (2017) 205–215. https://doi.org/10.2174/1389557516666161013103408.

[7] H. Potschka, Targeting regulation of ABC efflux transporters in brain diseases: A novel therapeutic approach, Pharmacol. Ther. 125 (2010) 118–127. https://doi.org/10.1016/j.pharmthera.2009.10.004.

[8] H. Potschka, H. Luna-Munguia, CNS Transporters and Drug Delivery in Epilepsy, Curr. Pharm. Des. 20 (2014) 1534–1542. https://doi.org/10.2174/13816128113199990461.

[9] A. Rosillo-de la Torre, Pharmacoresistant epilepsy and nanotechnology, Front. Biosci. E6 (2014) 329. https://doi.org/10.2741/709.

[10] A. Talevi, L.E. Bruno-Blanch, On the development of new antiepileptic drugs for the treatment of pharmacoresistant epilepsy: Different approaches to different hypothesis, in: L. Rocha, E.A. Cavalheiro (Eds.), Pharmacoresistance Epilepsy From Genes Mol. to Promis. Ther., 1st ed., Springer New York, New York, NY, 2013: pp. 207–224. https://doi.org/10.1007/978-1-4614-6464-8_14.

[11] S. Scioli Montoto, M.L. Sbaraglini, A. Talevi, M. Couyoupetrou, M. Di Ianni, G.O. Pesce, V.A. Alvarez, L.E. Bruno-Blanch, G.R. Castro, M.E. Ruiz, G.A. Islan, Carbamazepine-loaded solid lipid nanoparticles and nanostructured lipid carriers: Physicochemical characterization and in vitro/in vivo evaluation, Colloids Surfaces B Biointerfaces. 167 (2018). https://doi.org/10.1016/j.colsurfb.2018.03.052.

[12] G.A. Islan, M.L. Cacicedo, B. Rodenak-Kladniew, N. Duran, G.R. Castro, Development and Tailoring of Hybrid Lipid Nanocarriers, Curr. Pharm. Des. 167 (2018) 73–81. https://doi.org/10.2174/1381612823666171115110639.

[13] B. García-Pinel, C. Porras-Alcalá, A. Ortega-Rodríguez, F. Sarabia, J. Prados, C. Melguizo, J.M. López-Romero, Lipid-based nanoparticles: Application and recent advances in cancer treatment, Nanomaterials. 9 (2019) 638. https://doi.org/10.3390/nano9040638.

[14] R.H. Müller, K. Mäder, S. Gohla, Solid lipid nanoparticles (SLN) for controlled drug delivery - A review of the state of the art, Eur. J. Pharm. Biopharm. 50 (2000) 161–177. https://doi.org/10.1016/S0939-6411(00)00087-4.

[15] K.W. Kasongo, R.H. Mller, R.B. Walker, The use of hot and cold high pressure homogenization to enhance the loading capacity and encapsulation efficiency of nanostructured lipid carriers for the hydrophilic antiretroviral drug, didanosine for potential administration to paediatric patients, Pharm. Dev. Technol. 17 (2012) 353–362. https://doi.org/10.3109/10837450.2010.542163.

[16] B. Rodenak-Kladniew, S. Scioli Montoto, M.L. Sbaraglini, M. Di Ianni, M.E. Ruiz, A. Talevi, V.A. Alvarez, N. Durán, G.R. Castro, G.A. Islan, Hybrid Ofloxacin/eugenol co-loaded solid lipid nanoparticles with enhanced and targetable antimicrobial properties, Int. J. Pharm. (2019) 13. https://doi.org/https://doi.org/10.1016/j.ijpharm.2019.118575.

[17] C. Gunawan, M. Lim, C.P. Marquis, R. Amal, Nanoparticle-protein corona complexes govern the biological fates and functions of nanoparticles, J. Mater. Chem. B. 2 (2014) 2060–2083. https://doi.org/10.1039/c3tb21526a.

[18] J. Lazarovits, Y.Y. Chen, E.A. Sykes, W.C.W. Chan, Nanoparticle-blood interactions: The implications on solid tumour targeting, Chem. Commun. 51 (2015) 2756–2767. https://doi.org/10.1039/c4cc07644c.

[19] P. Aggarwal, J.B. Hall, C.B. McLeland, M.A. Dobrovolskaia, S.E. McNeil, Nanoparticle interaction with plasma proteins as it relates to particle biodistribution, biocompatibility and therapeutic efficacy, Adv. Drug Deliv. Rev. 61 (2009) 428–437. https://doi.org/10.1016/j.addr.2009.03.009.

[20] T.W. May, E. Korn-Merker, B. Rambeck, Clinical pharmacokinetics of oxcarbazepine, Clin. Pharmacokinet. 42 (2003) 1023–1042. https://doi.org/10.2165/00003088-200342120-00002.

[21] C. Zhang, Z. Zuo, P. Kwan, L. Baum, In vitro transport profile of carbamazepine, oxcarbazepine, eslicarbazepine acetate, and their active metabolites by human P-glycoprotein, Epilepsia. 52 (2011) 1894–1904. https://doi.org/10.1111/j.1528-1167.2011.03140.x.

[22] P.L. Ritger, N.A. Peppas, A simple equation for description of solute release I. Fickian and non-fickian release from non-swellable devices in the form of slabs, spheres,

cylinders or discs, J. Control. Release. (1987). https://doi.org/10.1016/0168-3659(87)90034-4.

[23] A. Lopalco, H. Ali, N. Denora, E. Rytting, Oxcarbazepine-loaded polymeric nanoparticles: development and permeability studies across in vitro models of the blood-brain barrier and human placental trophoblast, Int. J. Nanomedicine. 10 (2015) 1985–1996. https://doi.org/10.2147/IJN.S77498.

[24] T. Musumeci, M.F. Serapide, R. Pellitteri, A. Dalpiaz, L. Ferraro, R. Dal Magro, A. Bonaccorso, C. Carbone, F. Veiga, G. Sancini, G. Puglisi, Oxcarbazepine free or loaded PLGA nanoparticles as effective intranasal approach to control epileptic seizures in rodents, Eur. J. Pharm. Biopharm. 133 (2018) 309–320. https://doi.org/10.1016/j.ejpb.2018.11.002.

[25] G.M. El-Zaafarany, M.E. Soliman, S. Mansour, G.A.S. Awad, Identifying lipidic emulsomes for improved oxcarbazepine brain targeting: In vitro and rat in vivo studies, Int. J. Pharm. 503 (2016) 127–140. https://doi.org/10.1016/j.ijpharm.2016.02.038.

[26] G. El-Zaafarany, M. Soliman, S. Mansour, M. Cespi, G. Palmieri, L. Illum, L. Casettari, G. Awad, A Tailored Thermosensitive PLGA-PEG-PLGA/Emulsomes Composite for Enhanced Oxcarbazepine Brain Delivery via the Nasal Route, Pharmaceutics. 10 (2018) 217. https://doi.org/10.3390/pharmaceutics10040217.

[27] R. Ana, M. Mendes, J. Sousa, A. Pais, A. Falcão, A. Fortuna, C. Vitorino, Rethinking carbamazepine oral delivery using polymer-lipid hybrid nanoparticles, Int. J. Pharm. 554 (2019) 352–365. https://doi.org/10.1016/j.ijpharm.2018.11.028.

[28] M. Elmowafy, K. Shalaby, M.M. Badran, H.M. Ali, M.S. Abdel-Bakky, H.M. Ibrahim, Multifunctional carbamazepine loaded nanostructured lipid carrier (NLC) formulation, Int. J. Pharm. 550 (2018) 359–371. https://doi.org/10.1016/j.ijpharm.2018.08.062.

[29] V. Venkateswarlu, K. Manjunath, Preparation, characterization and in vitro release kinetics of clozapine solid lipid nanoparticles, J. Control. Release. 95 (2004) 627–638. https://doi.org/10.1016/j.jconrel.2004.01.005.

[30] D.A. Volpe, Drug-permeability and transporter assays in Caco-2 and MDCK cell lines, Future Med. Chem. 3 (2011) 2063–2077. https://doi.org/10.4155/fmc.11.149.

[31] H. Glavinas, P. Krajcsi, J. Cserepes, B. Sarkadi, The Role of ABC Transporters in Drug Resistance, Metabolism and Toxicity, Curr. Drug Deliv. 1 (2004) 27–42. https://doi.org/10.2174/1567201043480036.

[32] The United States Pharmacopeia 34, United States Pharmacopeia Convention, Rockville, 2011.

[33] Y. Zhang, M. Huo, J. Zhou, A. Zou, W. Li, C. Yao, S. Xie, DDSolver: An add-in program for modeling and comparison of drug dissolution profiles, AAPS J. 12 (2010) 263–271. https://doi.org/10.1208/s12248-010-9185-1.

[34] G.T. Hermanson, Bioconjugate Techniques: Third Edition, Elsevier Inc., 2013. https://doi.org/10.1016/C2009-0-64240-9.

[35] K.M. Lutker, A.J. Matzger, Crystal polymorphism in a carbamazepine derivative: Oxcarbazepine, J. Pharm. Sci. 99 (2010) 794–803. https://doi.org/10.1002/jps.21873.

[36] FDA Guidance for Industry: Q3C Impurities: Residual Solvents Appendix 6 - ECA Academy, (n.d.). http://www.gmp-compliance.org/guidelines/gmp-guideline/fda-guidance-for-industry-q3c-impurities-residual-solvents-appendix-6 (accessed July 9, 2019).

[37] G. Poovi, N. Damodharan, Lipid nanoparticles: A challenging approach for oral delivery of BCS Class-II drugs, Futur. J. Pharm. Sci. (2018). https://doi.org/10.1016/J.FJPS.2018.04.001.

[38] J. Zhang, Y. Fan, E. Smith, Experimental design for the optimization of lipid nanoparticles, J. Pharm. Sci. 98 (2009) 1813–1819. https://doi.org/10.1002/jps.21549.

[39] S. Das, A. Chaudhury, Recent advances in lipid nanoparticle formulations with solid matrix for oral drug delivery., AAPS PharmSciTech. 12 (2011) 62–76. https://doi.org/10.1208/s12249-010-9563-0.

[40] S.A. El-Gizawy, G.M. El-Maghraby, A.A. Hedaya, Formulation of acyclovir-loaded solid lipid nanoparticles: design, optimization, and in-vitro characterization, Pharm. Dev. Technol. 24 (2019) 1287–1298. https://doi.org/10.1080/10837450.2019.1667385.

[41] C. Lourenco, M. Teixeira, S. Simões, R. Gaspar, Steric stabilization of nanoparticles: Size and surface properties, Int. J. Pharm. 138 (1996) 1–12. https://doi.org/10.1016/0378-5173(96)04486-9.

[42] M.J. Santander-Ortega, A.B. Jódar-Reyes, N. Csaba, D. Bastos-González, J.L. Ortega-Vinuesa, Colloidal stability of Pluronic F68-coated PLGA nanoparticles: A variety of stabilisation mechanisms, J. Colloid Interface Sci. 302 (2006) 522–529. https://doi.org/10.1016/j.jcis.2006.07.031.

[43] C. Costa, J.N. Moreira, M.H. Amaral, J.M. Sousa Lobo, A.C. Silva, Nose-to-brain delivery of lipid-based nanosystems for epileptic seizures and anxiety crisis, J. Control. Release. 295 (2019) 187–200. https://doi.org/10.1016/j.jconrel.2018.12.049.

[44] T.B. Soares, L. Loureiro, A. Carvalho, M.E.C.D.R. Oliveira, A. Dias, B. Sarmento, M. Lúcio, Lipid nanocarriers loaded with natural compounds: Potential new therapies for age

related neurodegenerative diseases?, Prog. Neurobiol. 168 (2018) 21–41. https://doi.org/10.1016/j.pneurobio.2018.04.004.

[45] M. Lúcio, C.M. Lopes, E. Fernandes, H. Gonęalves, M.E.C.D. Real Oliveira, Organic Nanocarriers for Brain Drug Delivery, in: C. Vitorino, A. Jorge, A. Pais (Eds.), Nanoparticles Brain Drug Deliv., 1st ed., Jenny Stanford Publishing, New York, NY, 2020: pp. 75–160. https://doi.org/10.1201/9781003119326-6.

[46] T.G.F. Souza, V.S.T. Ciminelli, N.D.S. Mohallem, A comparison of TEM and DLS methods to characterize size distribution of ceramic nanoparticles, J. Phys. Conf. Ser. 733 (2016) 5. https://doi.org/10.1088/1742-6596/733/1/012039.

[47] W.J. Conover, Some Methods Based on Ranks, in: W.J. Conover (Ed.), Pract. Nonparametric Stat., 3rd ed., John Wiley & Sons, Inc., New York, NY, 1999: pp. 269–427.

[48] N.A. Peppas, B. Narasimhan, Mathematical models in drug delivery: How modeling has shaped the way we design new drug delivery systems, J. Control. Release. (2014). https://doi.org/10.1016/j.jconrel.2014.06.041.

[49] P. Costa, J.M. Sousa Lobo, Modeling and comparison of dissolution profiles, Eur. J. Pharm. Sci. 13 (2001) 123–133. https://doi.org/10.1016/S0928-0987(01)00095-1.

[50] M.L. Bruschi, Mathematical models of drug release, in: M.L.B.T.-S. to M. the D.R. from P.S. Bruschi (Ed.), Strateg. to Modify Drug Release from Pharm. Syst., 1st ed., Woodhead Publishing, New York, NY, 2015: pp. 63–86. https://doi.org/https://doi.org/10.1016/C2014-0-02342-8.

[51] J. Xue, T. Wang, Q. Hu, M. Zhou, Y. Luo, A novel and organic solvent-free preparation of solid lipid nanoparticles using natural biopolymers as emulsifier and stabilizer, Int. J. Pharm. 531 (2017) 59–66. https://doi.org/10.1016/j.ijpharm.2017.08.066.

[52] A. Zur Mühlen, C. Schwarz, W. Mehnert, Solid lipid nanoparticles (SLN) for controlled drug delivery - Drug release and release mechanism, Eur. J. Pharm. Biopharm. 45 (1998) 149–155. https://doi.org/10.1016/S0939-6411(97)00150-1.

[53] S. Scioli Montoto, M.L.M.L.M.L.L. Sbaraglini, A. Talevi, M. Couyoupetrou, M. Di Ianni, G.O.G.O.G.O.O. Pesce, V.A.V.A. Alvarez, L.E.L.E.L.E. Bruno-Blanch, G.R.G.R. Castro, M.E.M.E.M.E.E. Ruiz, G.A.G.A.A. Islan, Carbamazepine-loaded solid lipid nanoparticles and nanostructured lipid carriers: Physicochemical characterization and in vitro/in vivo evaluation, Colloids Surfaces B Biointerfaces. 167 (2018) 73–81. https://doi.org/10.1016/j.colsurfb.2018.03.052.

[54] X. Mulet, B.J. Boyd, C.J. Drummond, Advances in drug delivery and medical imaging

using colloidal lyotropic liquid crystalline dispersions, J. Colloid Interface Sci. 393 (2013) 1–20. https://doi.org/10.1016/j.jcis.2012.10.014.

[55] M.E. Di Ianni, G.A. Islan, C.Y. Chain, G.R.G.R. Castro, A. Talevi, M.E. Vela, Interaction of Solid Lipid Nanoparticles and Specific Proteins of the Corona Studied by Surface Plasmon Resonance, J. Nanomater. 2017 (2017) 1–11. https://doi.org/10.1155/2017/6509184.

Tables

Scioli Montoto et al.

Table 1. Composition of different NLC obtained by melt emulsification/ ultrasonication technique.

	Lipid Phase					Aqueous Phase		
	Crodamol CP (mg)	Oleic Acid (µL)	PG (mL)	DMSO (µL)	OXC (mg)	Kolliphor P188 (mg)	mCh (mg)	PVA (mg)
Oxcarbazepine loaded NLC[*]								
NLC-P188	400	112	2	50	60	600	–	–
NLC-PVA	400	112	2	50	60	500	–	100
NLC-mCh	400	112	2	50	60	500	100	–
Non-loaded NLC[*]								
NLC-P188	400	112	2	50	–	600	–	–
NLC-PVA	400	112	2	50	–	500	–	100
NLC-mCh	400	112	2	50	–	500	100	–

* Final volume of 20 ml.

Table 2. Particle Size (PS), polydispersity index (PI), zeta potential (ζ) and Entrapment Efficiency (EE%) of different formulations of NLC. Mean (and sd) of 3 determinations are presented.

	PS (nm)	PI	ζ (mV)	EE%	DL%
Oxcarbazepine loaded NLC					
NLC-P188	122.4 *(0.3)*	0.282 *(0.010)*	-1.68 *(0.79)*	97.5	14.6
NLC-PVA	162.6 *(1.1)*	0.262 *(0.007)*	-2.50 *(0.18)*	97.5	14.5
NLC-mCh	206.4 *(2.1)*	0.282 *(0.006)*	26.5 *(1.1)*	96.9	14.5
Non-loaded NLC					
NLC-P188	121.8 *(1.4)*	0.251 *(0.009)*	-3.23 *(0.16)*	–	–

NLC-PVA	154.6 *(1.2)*	0.248 *(0.001)*	-2.49 *(0.20)*	–	–
NLC-mCh	212.3 *(1.0)*	0.271 *(0.009)*	24.1 *(1.3)*	–	–

Table 3. Goodness-of-fit measures used as model selection criteria for fitting of the *in vitro* release profiles of OXC from NLC systems. *MSE = mean squared error; AIC = Akaike's information criteria; F= fraction dissolved (%).*

	Rsqr	***Rsqr-adj***	***MSE***	***AIC***	***Resid. sum***
Higuchi model - $F = k_H \cdot t^{0.5}$					
NLC-P188	0.983	0.983	0.94	8.60	-3.16
NLC-PVA	0.948	0.948	12.17	20.85	-13.02
NLC-mCh	0.966	0.966	5.91	17.79	-9.78
Korsmeyer-Peppas model - $F = k_{KP} \cdot t^n$					
NLC-P188	0.988	0.986	0.66	7.88	-0.65
NLC-PVA	0.979	0.976	4.70	4.10	0.37
NLC-mCh	0.997	0.997	0.53	11.58	-0.27
Baker-Londsdale model - $\frac{3}{2}\left[1-\left(\frac{100-F}{100}\right)^{2/3}\right]-\frac{F}{100}=k_{BL}\cdot t$					
NLC-P188	0.979	0.979	1.12	9.49	-5.58
NLC-PVA	0.910	0.910	21.61	23.23	-22.82
NLC-mCh	0.955	0.955	7.92	19.27	-4.93

Table 4. Parameters estimation for the best fitting model (Korsmeyer-Peppas).

	k_{KP}			n		
	Est.	SE	p-value	Est.	SE	p-value
NLC-P188	4.15	0.38	<0.0001	0.58	0.04	<0.0001
NLC-PVA	5.23	0.95	0.0006	0.76	0.08	<0.0001
NLC-mCh	5.63	0.33	<0.0001	0.69	0.03	<0.0001

Abbreviations: SE: standard error; k_{KP}*: Korsmeyer-Peppas model constant; n: model exponent.*

Table 5. Mean angular shifts (Δθ) achieved to estimate the surface coverage (Γp), hydrodynamic diameters (Dh) and molecular weights (MW) employed to calculate the close packed coverage (Γp*)

Protein	$\Delta\vartheta$ [deg]	D_h [nm]	MW [kDa]	Γ_p [ng/cm^2]	Γ_p* [ng/cm^2]	Γ_p/Γ_p* [%]
BSA	0.133	5.3	66.5	139	453	31
IgG	0.083	7.0	150	87	590	15
IgM	0.287	13.2	990	302	1060	28

Figures

Scioli Montoto *et al*.

Figure 1. Images obtained through TEM of ANLC-P188 (A), NLC-PVA (B), and NLC-mCh (C).

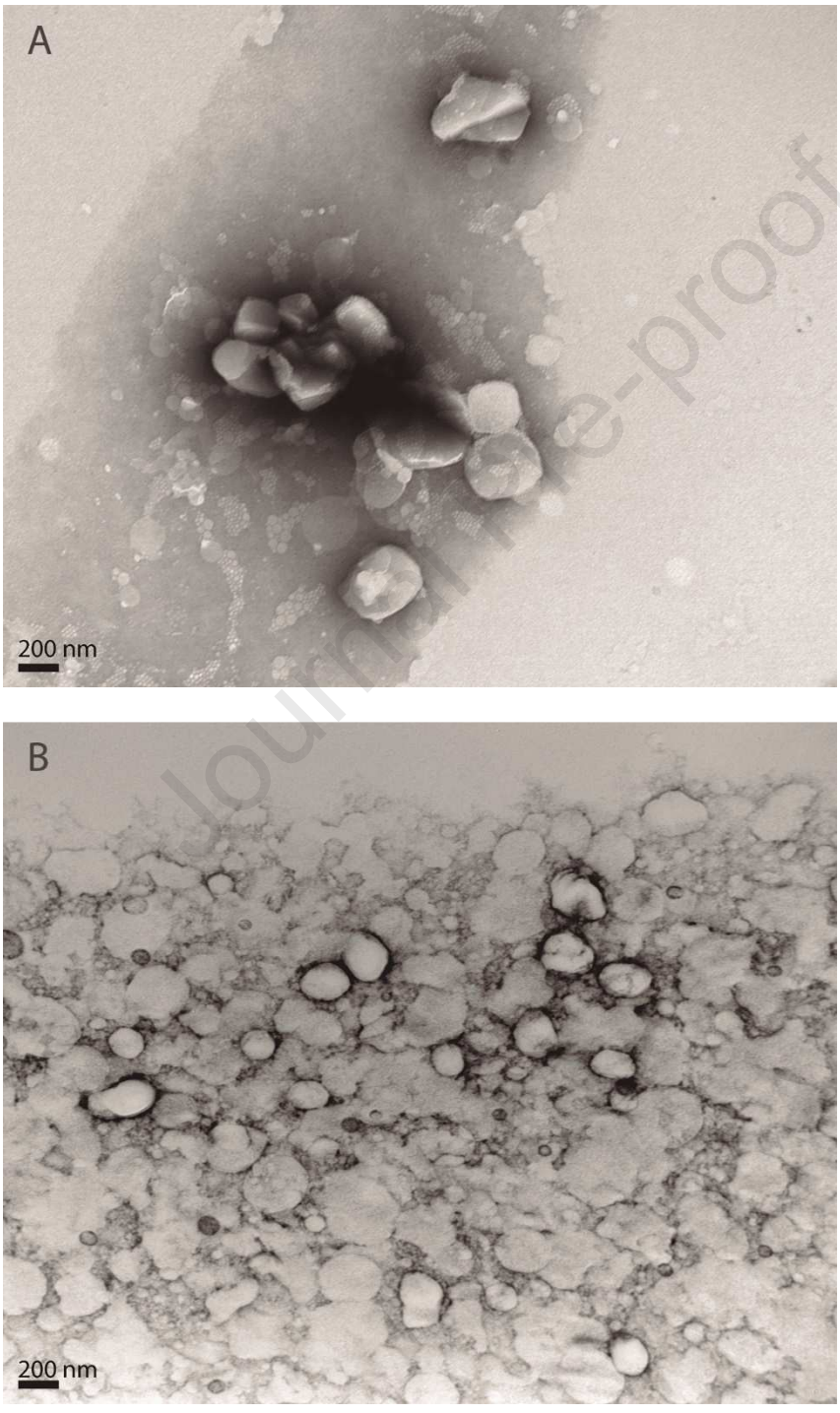

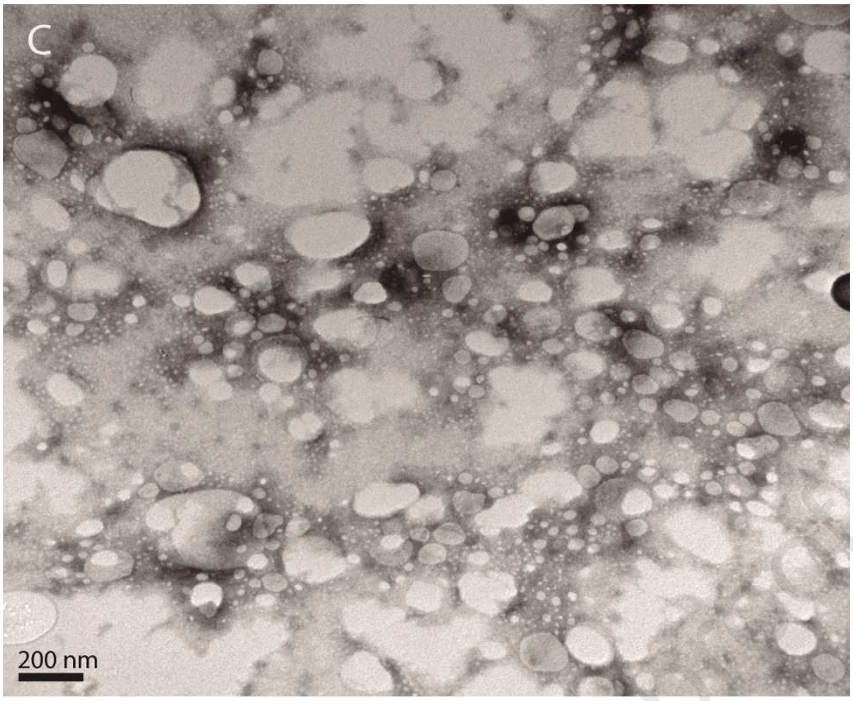

Figure 2. Release profiles of NLC-P188, NLC-PVA, NLC-mCh, and free OXC. Each experimental point represents the mean ± SD values of two independent determinations.

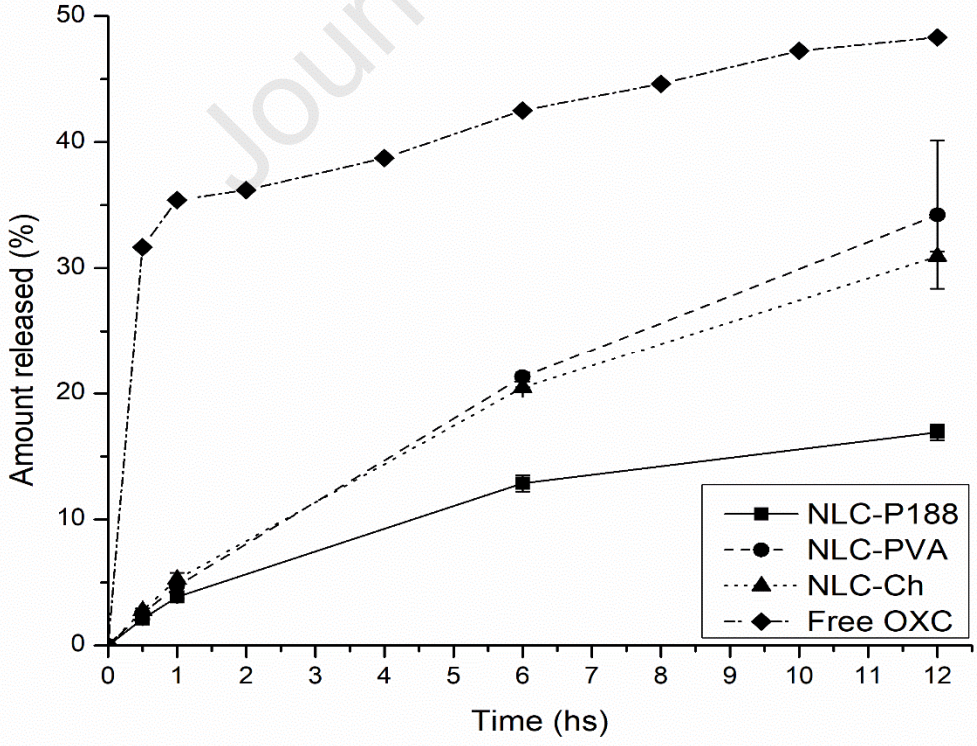

Figure 3. Sensorgrams showing the SPR signal resulting from the injection of non-loaded NLC (a, c) and oxcarbazepine loaded NLC (b, d) onto the control surface. Each cycle included a ten-minute injection of the NLC suspension followed by a washing step with PBS (pH= 7.4). ΔΘSPR corresponding to each NLC measured at 730 s of each cycle (arrows). Symbols: control (¯¯), immobilized IgM (■), BSA (□), and IgG (▲), respectively.

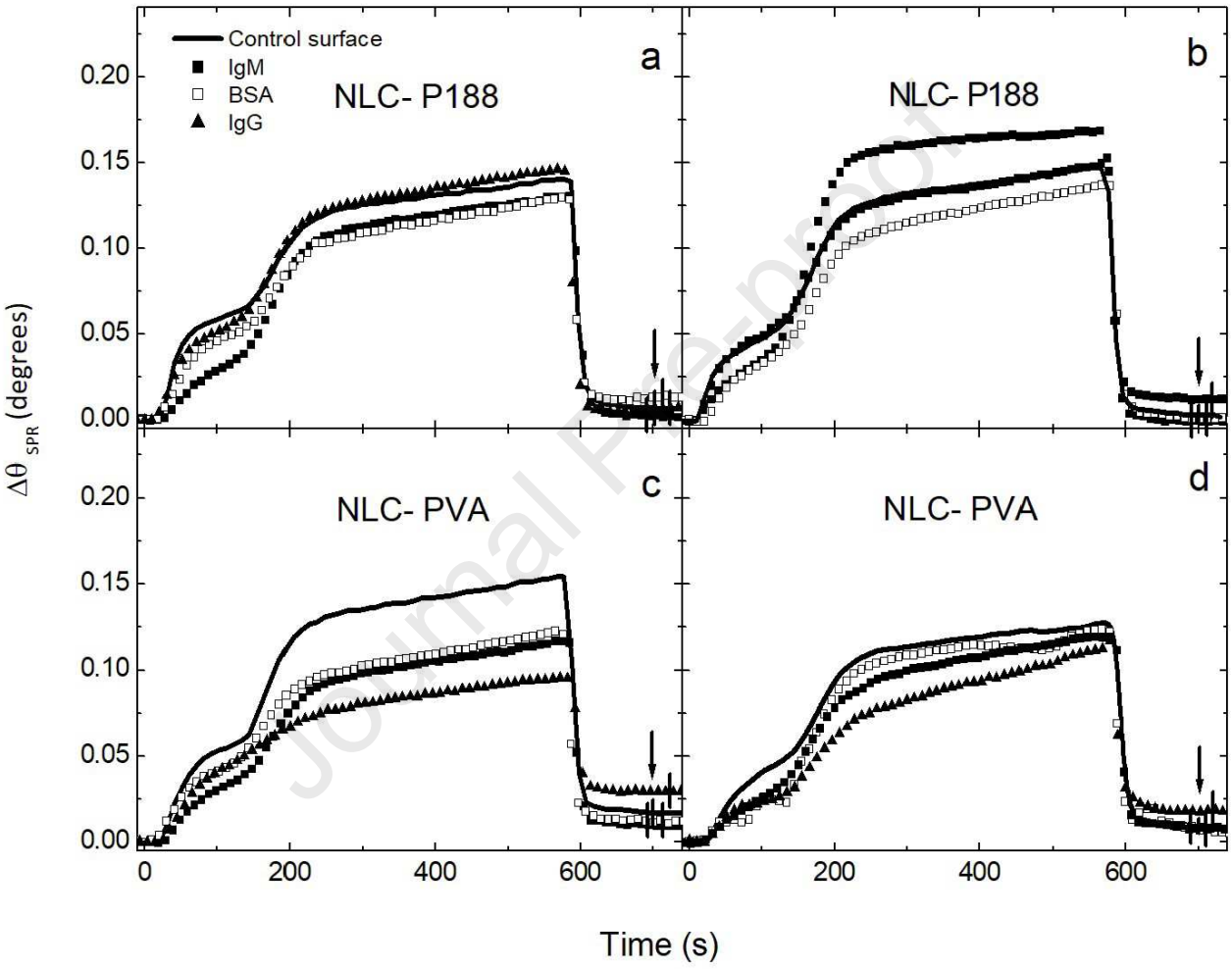

HIGHLIGHTS

- Oxcarbazepine (OXC) is a class II AED used for both focal and generalized seizures
- Development nanostructured lipid carriers for oxcarbazepine delivery.
- NLC coated with PVA and chitosan displayed physicochemical properties
- Enhanced permeability in MDCK-MDR1 cells was found with OXC loaded in NLC.
- No interaction between NLCs and blood proteins were observed by SPR experiments

CONFLICT OF INTEREST

The authors confirm that this article content has no conflicts of interest.